Rapid inner-volume imaging in the steady-state with 3D selective excitation and small-tip fast recovery (STFR) imaging

HAO SUN[1], JEFFREY A. FESSLER[1,2],
DOUGLAS C. NOLL[2], AND JON-FREDRIK NIELSEN[2,*]

Departments of [1]Electrical Engineering and Computer Science and [2]Biomedical Engineering, University of Michigan, Ann Arbor, MI, USA

Journal: Magnetic Resonance in Medicine
Article type: Note
Running Head: reduced FOV STFR
Word count: 2791
Grant Funding: National Institutes of Health R21EB019653

* Correspondence to:
Jon-Fredrik Nielsen, PhD
Department of Biomedical Engineering
University of Michigan
1067 B.I.R.B.
2360 Bonisteel Ave
Ann Arbor, MI 48109 - 2108
Email: jfnielse@umich.edu

Abstract

Purpose: Develop a method for rapid 3D inner-volume (IV), or reduced field-of-view (rFOV), steady-state imaging.

Methods: Tailored radiofrequency pulses for exciting a 3D IV were designed using a recently proposed algorithm and used in three different sequences: spoiled gradient echo (SPGR), balanced steady-state free precession (bSSFP), and "small-tip fast recovery" (STFR) which uses a "tip-up" RF pulse after the readout to fast recover spins to the longitudinal axis. The inner- and outer-volume (OV) steady-state signals were analyzed. To demonstrate the potential utility of the proposed method, segmented stack-of-spirals rFOV images in a volunteer were acquired.

Results: For a given 3D IV excitation pulse, STFR can achieve higher IV/OV signal ratio compared to SPGR and bSSFP. For SPGR and bSSFP this ratio is significantly lower than that produced by a single IV excitation. For STFR this ratio *exceeds* that produced by a single IV excitation, due to partial OV saturation produced by the non spatially selective tip-up pulse. Reduced FOV STFR stack-of-spirals imaging with 2-fold under-sampling in both x-y and z is demonstrated.

Conclusion: STFR provides an effective mechanism for OV suppression in steady-state IV imaging. The recently proposed joint pulse design method can be used in the STFR sequence to achieve fast rFOV imaging.

Introduction

In inner-volume imaging (IVI), a 2D or 3D sub-volume is excited within the object such that only a reduced field of view (rFOV) needs to be encoded. Ideally, the 3D IV is directly excited with a short radiofrequency (RF) pulse, and a "tight" (e.g., non-Cartesian) readout trajectory that matches the rFOV is used. For example, a cylindrical IV ("hockey puck") can be read out efficiently with a 3D stack-of-spirals readout. However, a 3D selective pulse with non-smooth target pattern can be prohibitively long. Therefore, most existing IVI methods are 2D selective, using spin echo or 2D excitation pulses. The typical spin echo IVI method in (1) uses a 90^{o} slice-selective pulse followed by a 180^{o} slice-selective pulse in a perpendicular direction. Only spins inside the "pencil beam" excited by both RF pulses are refocused and generate signal. One can limit the FOV in the unrestricted dimension by using a Cartesian readout with frequency encoding along the pencil beam direction with a low pass filter. In some other methods, a 2D selective pulse is transmitted to directly excite a column, with the FOV in the third dimension restricted with frequency encoding or other special readout techniques (2–6). Unfortunately, using frequency-encoding along one dimension limits the choice of data sampling in the other two dimensions to simple phase-encoding which is slow compared to non-Cartesian readouts. For this reason, 2D RF pulses are often not compatible with fast 3D non-Cartesian readouts, unless the FOV in the 3rd dimension can be restricted by other means, e.g., by exploiting local coil sensitivities.

Parallel transmit (PTx) methods have been proposed recently for IVI with 3D selective excitation (7–9). In (7) a 3.2 ms IV pulse was demonstrated with an 8-channel PTx system, but using a preclinical scanner with gradient specs (660 mT/m maximum amplitude; 5600 T/m/s maximum slew rate) that far exceed the capability of clinical systems. PTx experiments on human scanners have reported IVI pulses of duration 12.0–14.9 ms (8,9) that are too long for rapid steady-state imaging. Moreover, parallel excitation requires specialized hardware that is not widely available.

Here we propose a novel implementation of IV imaging, based on (i) 3D selective excitation using a recently proposed joint RF/gradient pulse design approach (10,11), and (ii) the small-tip fast recovery (STFR) steady-state imaging sequence (12–15). The advantage of 3D IV excitation (over 2D) is that it allows arbitrary non-Cartesian 3D readouts and hence rapid imaging. With this approach we demonstrate steady-state imaging with 3D IV excitation using a short ($\sim$1.5–4.0 ms) RF pulse on a standard clinical scanner equipped with single-channel excitation. We show that STFR achieves

a higher inner- to outer-volume signal ratio compared to the single shot excitation ratio, spoiled gradient-echo imaging (SPGR; fast low angle shot, or FLASH; T1-fast field echo, or T1-FFE), and balanced steady-state free precession (bSSFP).

Theory: outer-volume signal suppression in STFR

STFR is a steady-state sequence having a "tip-up" (or fast recovery) RF pulse to preserve the magnetization in the longitudinal direction after readout (12–15). The tip-up pulse can be either a spatial (12–14), spectral (15, 16), or spectral-spatial (17) pulse. The original motivation for STFR was to achieve bSSFP-like signal while mitigating banding artifacts; however in rFOV imaging only local shimming over the IV is needed and hence banding would occur much less frequently. The focus here is on the need to suppress OV signal, and we hypothesize that STFR is well suited for this.

Figure 1 shows the IV and OV spin paths for an idealized STFR sequence, i.e., assuming tip-down and tip-up pulses of negligible duration that are perfectly matched to the local off-resonance. IV spins experience both tip-down and tip-up pulses, whereas OV spins mainly experience the non spatially selective tip-up pulse. The resulting steady-state signal for IV spins can be bSSFP-like (13, 15). The central point here is that the tip-up pulse helps to partially saturate OV spins, such that the steady-state OV signal resulting from non-ideal IV excitation is relatively small in STFR compared to the corresponding SPGR or bSSFP sequence (using the same IV excitation pulse).

Methods

RF pulse design

In (10) we proposed a method for the joint design of RF waveform and excitation k-space trajectory that improved accuracy over several existing 3D selective excitation designs (18,19). In particular, we excited a cube with $<$15% relative OV excitation using a 4 ms RF pulse and single-coil transmission. Our joint design is an extension of the KT-points method (18), and is summarized in Fig. 2 and Algorithm 1.

Algorithm 1 Extended KT-points RF pulse design

1: Find phase encoding locations using method (20).
2: Locally optimize those phase encoding locations using Levenberg-Marquardt algorithm (21).
3: Find the optimal visiting order using traveling salesman algorithm (22).
4: Generate the fastest gradient waveform using (23).
5: Generate the final RF pulse using iterative small-tip pulse design (24).

Simulation and imaging experiments

To evaluate the ability of STFR to improve the IV/OV signal ratio relative to SPGR and bSSFP, we simulated the steady-state IV and OV signal for a range of tip-down and tip-up angles (1–60^{o}), using T1/T2 values for white matter (1.10/0.06 sec) and cerebrospinal fluid (CSF) (4.0/2.0 sec) (25). TR was 10 ms for all sequences. Based on simulations of our 3D IV pulses (e.g., Fig. 5(a)), we assumed that the 3D IV excitation pulse produced a maximum residual magnetization in the OV equal to 15% of the IV transverse magnetization (after a single excitation). For bSSFP we assumed on-resonance conditions, i.e., we did not evaluate the signal near band edges or in neighboring bands. For IV spins this assumption is reasonable since a reduced FOV can often be shimmed accurately, however for OV spins this assumption is not satisfied in general. The OV steady-state signal for bSSFP can vary strongly near band edges and can be either larger or smaller than the on-resonance signal depending on the off-resonance and flip angle. Since the bSSFP signal for low flip angles (as found in the OV region) is generally lowest on-resonance , the on-resonance assumption used here generally leads to a best-case estimate of the IV/OV ratio for bSSFP.

Imaging experiments were done on a GE 3T scanner equipped with a quadrature transmit/receive head coil and standard gradients (50 mT/m amplitude and 150 mT/m/ms slew rate design limits), using IRB approved protocols. The flip angles reported are those of the center pixel in the IV region as determined by Bloch simulation of the IV excitation pulses . Two *in vivo* steady-state imaging experiments were performed. In the first experiment we evaluated the IV/OV signal ratio quantitatively for RF-spoiled STFR, SPGR, and bSSFP, using a rectangular box IV excitation and Cartesian readout. RF-spoiling is needed in inner-volume STFR imaging to suppress the SSFP-echo signal in the OV region produced by the (spatially non-selective) tip-up pulse (12). In each TR, the IV excitation pulse and the tip-up pulse had a common transmitter phase offset that evolved quadratically as in standard RF-spoiling (26). Both SPGR and STFR used a linear RF spoiling increment

factor of 117°. We also acquired conventional bSSFP data for reference. A 4 ms 3D RF pulse was designed to excite a 6x6x3 cm^3 rectangular box IV with flip angle 11°. All sequences used the same 3D Cartesian readout (192x192x42 matrix; 24x24x21 cm^3 FOV). The IVex-STFR sequence (Figure 1(c)) used a spectral pre-winding tip-up pulse targeted to -30 to 30 Hz (15, 16). The relative RF energy for the IV excitation and spectral tip-up pulse was 0.71 and 1.04, respectively, compared to a 1.25 ms 30° Shinnar-Le Roux (SLR) pulse of time-bandwidth product four. Thus, the RF energy per TR for the STFR sequence was 1.75 times higher than a corresponding bSSFP sequence. We used auto-prescan to properly shim the IV. The repetition times (TRs) of SPGR/bSSFP/STFR were 8.5/7.6/10.5 ms, respectively. To confirm that the tip-up pulse enhances the steady-state signal relative to SPGR, and to verify that STFR and bSSFP signal levels are similar, the flip angles were 11° for SPGR and STFR (which is between the optimal angles for SPGR and STFR, as explained below) and 22° for bSSFP (STFR requires only half the flip angle compared to bSSFP).

In the second *in vivo* experiment we acquired rFOV images in a volunteer using non-Cartesian (3D stack-of-spirals) imaging, to demonstrate the potential utility of the proposed 3D IV imaging method. Such an rFOV sequence could be used for rapid high-resolution anatomical imaging in a region of interest (ROI). The 3D IV excitation was a 1.45 ms tailored RF pulse for exciting a short cylinder (hockey puck) of diameter 9 cm and height 6 cm, offset 4 cm in the A/P direction for visualizing frontal brain matter. The relative energy for this pulse was 0.12 times that of the 30° SLR reference pulse. We segmented the acquisition into 96 balanced 2D spiral-out leafs of duration 3.2 ms covering kx-ky, and 48 kz-encodes (supporting full FOV 24x24x24 cm^3 and full reconstructed matrix size 240x240x48). The STFR sequence used a 3 ms spectral tip-up pulse as described above. The sequence TRs and flip angles were 7.0/12.7 ms and 26°/13° for bSSFP/STFR, respectively. These are close to the optimal flip angles for gray matter at 3T (32°/16° for bSSFP/STFR, assuming T1/T2 = 1470/71 ms (25)). (The slight deviation from the theoretically optimal flip angles does not matter much since the steady-state signal curve as a function of flip angle is relatively flat near the optimum.) We performed each image acquisition twice, however due to subject motion only one bSSFP acquisition was used in the analysis. We reconstructed fully sampled and undersampled 3D images using inverse FFT and nonuniform FFT (27) in the through- and in-plane dimensions, respectively, implemented with the IRT Matlab toolbox (http://www.eecs.umich.edu/∼fessler). For the undersampled (rFOV) images we undersampled by a factor of two in-plane and a factor two through-plane, i.e., the rFOV data contained 48 spiral leafs and 24 kz-encodes and supported an rFOV of 12x12x12 cm^3.

Results

Figure 3 shows simulated IV and OV signals and their ratio for white matter and CSF. STFR achieves effective OV suppression with similar tip-down and tip-up angles, with a peak IV/OV ratio of 15.5 for white matter at tip-down/tip-up flip angles $15^o/17^o$ which exceeds the direct excitation ratio of 6.7 (1/0.15). The IV/OV ratio for bSSFP and SPGR is below 6.7, showing amplification of the OV signal. For the flip angles used in our first *in vivo* experiment ($11^o/11^o$), the simulated IV/OV ratio is 2.0/4.0/11.9 for SPGR/bSSFP/STFR, respectively. The flip angle that produces the best IV/OV ratio is much higher for CSF than for white matter, and the ratio for CSF reaches a much higher peak value. In other words, a single flip angle cannot simultaneously achieve optimal IV/OV ratio for all tissue types. For a flip angle of 21^o the IV/OV ratio for both tissue types is just above 14, which may be a good operating point in some applications.

Figure 4 shows *in vivo* experimental results obtained with a rectangular box IV excitation and Cartesian readout. The observed mean IV/OV ratio for SPGR/bSSFP/STFR is 2.4/4.0/12.4, respectively, consistent with our simulations (Fig. 3). The IV region in bSSFP and STFR shows similar tissue signal strength (including bright CSF), consistent with previous reports (12, 13). However the IVex-bSSFP images have undesired OV signal, especially near banding regions. This may be because bSSFP has high signal near the band edge for low flip angles. The OV signal in IVex-STFR is effectively suppressed. We think there are two reasons for this: first, the OV spins are partially suppressed by the tip-up pulse and RF spoiling, as explained previously and demonstrated in the simulation (Figure 3); second, STFR does not have the hyperintense signal behavior near band edges (15).

Figure 5 shows results from the rFOV stack-of-spirals imaging experiment, which used a hockey puck IV excitation with $<$15% relative OV direct excitation (Fig. 5(a)). The tip-up angle for the STFR acquisition was reduced slightly to 80% of the tip-down angle (i.e., 80% of 13^o) since we observed that this adjustment produced somewhat improved CSF/brain tissue contrast. By comparing the fully sampled and subsampled reconstructions (Figs. 5(c) and (d), bottom row) we conclude that STFR achieves the best OV suppression among these sequences.

Discussion

We have shown that the tip-up pulse in STFR provides a partial saturation mechanism for suppressing the relative OV steady-state signal, enhancing the IV/OV steady-state ratio relative to that of a single IV excitation. This is in contrast with SPGR or bSSFP that invariably produce IV/OV ratios below that of a single excitation. We believe this behavior makes STFR uniquely suited for steady-state 3D IV imaging, provided that a reasonably accurate 3D IV excitation pulse can be designed as shown here.

STFR relies on tip-up pulses that fast recover spins with reasonable accuracy within the IV, which may be difficult to achieve in applications having large B0 inhomogeneity within the IV. In addition, designing the IV excitation pulse generally becomes more difficult with increasing object size, since the OV region becomes larger.

There may be several ways to reduce the direct OV excitation without compromising IV excitation accuracy significantly. First, since the steady-state signal is relatively insensitive to flip angle in the 10–20^{o} range , we may use a smaller weighting for the IV and a larger weighting for the OV in the pulse design cost function (28). Another possibility is to limit the maximum excitation error instead of the L2 norm of the error in the OV (29). Second, most of the excitation error occurs at the IV boundary where the target excitation pattern changes sharply, so the optimization algorithm may put more effort to minimize error in this region. However, excitation errors at the boundary are of minor consequence as long as the imaging FOV includes the boundary region, which means that less weight can be placed on this region during pulse design (28). Alternatively, one could smooth the target excitation pattern so the cost function is less dominated by boundary error. Finally, in addition to improving the 3D selective pulse itself to reduce OV signal, we could incorporate a slab-selective OV suppression pulse between the tip-up pulse and the gradient crusher to further suppress the OV signal.

In this paper we used the same IV pulse for all sequence types (SPGR/bSSFP/STFR), to support the key point that the tip-up pulse in STFR generally acts to improve the IV/OV signal ratio. However, it is generally desirable to optimize the IV excitation pulse with respect to the expected steady-state magnetization for each sequence, for a particular target tissue type. For example, when designing an IV pulse for SPGR it may be beneficial to place larger weight on the OV region, at the cost of less accurate IV excitation profile.

As stated above, the original motivation for STFR was to achieve bSSFP-like signal while mitigating banding artifacts, and in theory the ideal spectral-STFR signal is comparable to on-resonance bSSFP even when the spectral-STFR sequence is RF-spoiled (12, 13, 15). However, in Figs. 4 and 5 the observed image contrast for STFR and bSSFP is different and varies spatially, and we believe there are two main reasons for this. First, since the durations of the IV excitation (tip-down) and tip-up RF pulses are not small compared to the overall TR, significant T2 decay may occur during RF transmission, particularly during the spectral tip-up pulse (15). This would suppress white and gray matter signal relative to CSF in the STFR images, as observed in Fig. 5. Second, near the boundary of the IV region the tip-down angle is reduced, whereas the tip-up flip angle is not (since the tip-up pulse is not spatially selective). Such a mismatch in tip-down and tip-up angles would lead to a signal drop and loss of tissue contrast in STFR, as observed near the boundary of the IV region in Fig. 5.

Another factor affecting the tradeoff between STFR and bSSFP is SNR efficiency. The sequence TR of STFR is necessarily longer than the corresponding bSSFP sequence due to the insertion of an additional RF pulse and an unbalanced gradient (after the tip-up pulse), and STFR therefore has intrinsically lower SNR efficiency than bSSFP. This is a drawback of the proposed method, and should be weighed against the benefit of improved IV/OV ratio with STFR for a given application and IV excitation pulse.

Conclusion

The inner- to outer-volume steady-state signal ratio in rFOV STFR imaging exceeds that of a single excitation, indicating that STFR contains an effective mechanism for outer-volume signal suppression. Reduced FOV steady-state imaging without the tip-up pulse, e.g., bSSFP or SPGR, is challenging since the relative OV signal is amplified with these sequences.

References

1. Feinberg D, Hoenninger J, Crooks L, Kaufman L, Watts J, Arakawa M. Inner volume MR imaging: technical concepts and their application. Radiology 1985;156:743–747.

2. Hardy CJ, Cline HE. Spatial localization in two dimensions using NMR designer pulses. J Mag Res 1989;82:647–54.

3. Zhao L, Madore B, Panych LP. Reduced field-of-view MRI with two-dimensional spatially-selective RF excitation and UNFOLD. Magn Reson Med 2005;53:1118–25.

4. Stenger VA, Giurgi MS, Boada FE, Noll DC. Excitation UNFOLD (XUNFOLD) to improve the temporal resolution of multishot tailored RF pulses. Magn Reson Med 2006;56:692–697.

5. Yuan J, Zhao TC, Tang Y, Panych LP. Reduced field-of-view single-shot fast spin echo imaging using two-dimensional spatially selective radiofrequency pulses. J Magn Reson Imaging 2010; 32:242–248.

6. Mei CS, Panych LP, Yuan J, McDannold NJ, Treat LH, Jing Y, Madore B. Combining two-dimensional spatially selective RF excitation, parallel imaging, and UNFOLD for accelerated MR thermometry imaging. Magn Reson Med 2011;66:112–122.

7. Schneider JT, Kalayciyan R, Haas M, Herrmann SR, Ruhm W, Hennig J, Ullmann P. Inner-volume imaging in vivo using three-dimensional parallel spatially selective excitation. Magn Reson Med 2013;69:1367–1378.

8. Malik SJ, Hajnal JV. 3D-FSE Inner Volume Imaging using 3D selective excitation. In Proc. Intl. Soc. Magn. Reson. Med. 2014; 0948.

9. Haas M, Snyder J, Buchenau S, Kokorin D, Schneider JT, Ullmann P, Hennig J, Zaitsev M. Selective excitation of arbitrary three-dimensional targets in vivo using parallel transmit. In Proc. Intl. Soc. Magn. Reson. Med. 2012; 3476.

10. Sun H, Fessler JA, , Noll D, Nielsen JF. Joint design of continuous excitation k-space trajectory and RF pulse for 3D tailored excitation. In Proc. Intl. Soc. Magn. Reson. Med. 2014; 1438.

11. Sun H, Fessler JA, , Noll D, Nielsen JF. Joint design of excitation k-space trajectory and RF pulse for small-tip 3D tailored excitation in MRI. IEEE Trans Med Imaging 2015; doi:10.1109/TMI.2015.2478880.

12. Nielsen JF, Yoon D, Noll DC. Small-tip fast recovery imaging using non-slice-selective tailored tip-up pulses and radiofrequency-spoiling. Magn Reson Med 2013;69:657–666.

13. Sun H, Fessler JA, Noll D, Nielsen JF. Strategies for improved 3D Small-Tip Fast Recovery (STFR) imaging. Magn Reson Med 2014;72:389–398.

14. Sun H, Fessler JA, Noll DC, Nielsen JF. Steady-state functional MRI using spoiled small-tip fast recovery imaging. Magn Reson Med 2015;73:536–543.

15. Sun H, Fessler JA, Noll DC, Nielsen JF. Balanced SSFP-like steady-state imaging using small-tip fast recovery with a spectral prewinding pulse. Magn Reson Med 2015;doi: 10.1002/mrm.25682.

16. Asslander J, Glaser SJ, Hennig J. Spin echoes in the regime of weak dephasing. Magn Reson Med 2015;doi:10.1002/mrm.25579.

17. Williams S, Sun H, Nielsen JF, Fessler JA, Noll D. A spectral-spatial pulse for improved signal recovery in the small-tip fast recovery (STFR) sequence. In Proc. Intl. Soc. Magn. Reson. Med. 2015; 919.

18. Cloos M, Boulant N, Luong M, Ferrand G, Giacomini E, Le Bihan D, Amadon A. kT-points: Short three-dimensional tailored RF pulses for flip-angle homogenization over an extended volume. Magn Reson Med 2012;67:72–80.

19. Malik SJ, Keihaninejad S, Hammers A, Hajnal JV. Tailored excitation in 3D with spiral nonselective (SPINS) RF pulses. Magn Reson Med 2012;67:1303–15.

20. Yoon D, Fessler JA, Gilbert AG, Noll DC. Fast joint design method for parallel excitation RF pulse and gradient waveforms considering off-resonance. Magn Reson Med 2012;68:278–85.

21. Press WH, Flannery BP, Teukolsky SA, Vetterling WT. Numerical recipes in C. New York: Cambridge Univ. Press, 2 edition, 1992.

22. Kirk J. Traveling salesman program – genetic algorithm. `http://www.mathworks.com/matlabcentral/files/13680/tsp_ga.m`.

23. Lustig M, Kim SJ, Pauly JM. A fast method for designing time-optimal gradient waveforms for arbitrary-space trajectories. IEEE Trans Med Imaging 2008;27:866–873.

24. Yip C, Grissom WA, Fessler JA, Noll DC. Joint design of trajectory and RF pulses for parallel excitation. Magn Reson Med 2007;58:598–604.

25. Stanisz G, Odrobina E, Pun J, Escaravage M, Graham S, Bronskill M, Henkelman R. T_1, T_2 relaxation and magnetization transfer in tissue at 3T. Magn Reson Med 2005;54:507–512.

26. Zur Y, Wood ML, Neuringer LJ. Spoiling of transverse magnetization in steady-state sequences. Magn Reson Med 1991;21:251–263.

27. Fessler JA, Sutton BP. Nonuniform fast Fourier transforms using min-max interpolation. IEEE Trans Sig Proc 2003;51:560–74.

28. Yip C, Fessler JA, Noll DC. Iterative RF pulse design for multidimensional, small-tip-angle selective excitation. Magn Reson Med 2005;54:908–17.

29. Sun H, Weller DS, Chu A, Ramani S, Yoon D, Nielsen JF, Fessler JA. Spoke pulse design in magnetic resonance imaging using greedy minimax algorithm. In Biomedical Imaging (ISBI), 2013 IEEE 10th International Symposium on. IEEE, 2013; 696–699.

Figure 1: Proposed inner-volume-excitation STFR (IVex-STFR) sequence with 3D selective tip-down pulse (α) and spectral pre-winding tip-up pulse ($-\beta$). (a-b) Spin paths for (a) inner-volume (IV) and (b) outer-volume (OV) regions. (c) Schematic pulse sequence timing diagram. The IV excitation pulse tips the IV spins down toward the transverse plane (path 4$\rightarrow$1 in Fig. (a)), after which the spin precesses with off-resonance frequency ω (1$\rightarrow$2). After data readout, a non spatially selective tip-up pulse is played out, whose phase is nominally equal to the spin phase $\theta(\omega)$ such that the spin is tipped back toward the longitudinal axis (path 2$\rightarrow$3 in (a)). Outer-volume spins mainly experience the non spatially selective tip-up pulse (2$\rightarrow$3 in Fig. (b)). However, since the IV excitation pulse can never be perfect, some direct OV excitation from the tip-down pulse (4$\rightarrow$1) is inevitable. To avoid coherent steady-state signal from this small direct OV excitation, RF spoiling is used (12). The central point in this work is that the tip-up pulse in STFR helps to suppress the steady-state OV signal resulting from imperfect IV excitation pulses.

Figure 2: Summary of the 3D RF pulse design algorithm, first described in (10) and more recently in (11). We first obtain a KT-points trajectory (discrete "phase-encoding" locations in kx-ky-kz; blue "+" marks) using a modified orthogonal matching pursuit (OMP) approach (20). We then locally optimize the encoding locations using gradient-based algorithms (red triangles). We then determine the optimal visiting order for those phase encoding locations using a travelling salesman algorithm (22) (black straight line segments on left). Finally, we generate a continuous gradient waveform (right) that traverses those points using the method in (23), and design the RF pulse on this optimized k-space trajectory using iterative small-tip selective pulse design (28). In this example the target excitation is a rectangular box whose Fourier transform is a 3D sinc, and the final smooth k-space trajectory is concentrated in regions of 3D k-space where the Fourier transform of the target excitation is relatively large.

Figure 3: Simulated inner- and outer-volume steady-state signals and their ratio for STFR, bSSFP and SPGR. Results are shown for (a–f) white matter and (g–l) CSF. (a–c) STFR results for different tip-down and tip-up angle combinations, presented as 2D plots. Flip angles are in degrees. (d–f) Steady-state signal plots for SPGR and bSSFP, and for STFR with equal tip-down and tip-up angles. One-shot excitation in the outer-volume is 15$\%$ of the inner-volume, so an IV/OV steady state signal ratio larger than 1/0.15 ($=$6.7) means the sequence suppresses the OV signal, as seen for STFR. With the flip angles used in our first *in vivo* experiment (Fig. 4), the simulated IV/OV ratios for white matter is 2.0/4.0/11.9, for SPGR/bSSFP/STFR, respectively. (g–l) Corresponding results for CSF.

Figure 4: Steady-state brain imaging (a-c) with and (d) without inner-volume excitation, using a pulse sequence similar to that shown in Fig. 1(c). The target IV is a rectangular box. The gray scale is normalized by the maximum image value of each acquisition. The same eight slices are shown for (a) IVex-SPGR, (b) IVex-bSSFP, (c) IVex-STFR, (d) and conventional bSSFP. Balanced SSFP and STFR show similar tissue signal for inner-volume spins, but STFR has better OV suppression. The observed IV/OV ratios are 2.4/4.0/12.5 for IVex-SPGR/IVex-bSSFP/IVex-STFR, respectively, consistent with our simulations in Fig. 3.

Figure 5: Stack-of-spirals rFOV imaging results for bSSFP and STFR, using a short (1.45 ms) "hockey puck" IV excitation. (a) Simulated magnetization produced by a single application of the IV excitation pulse. Twelve slices are shown. The short RF pulse produces a relatively blurred excitation pattern compared to the longer (4 ms) IV pulse in Fig. 4. The peak OV/IV excitation ratio is about 15% for this RF pulse. (b) STFR pulse sequence diagram, showing actual waveforms and sequence timing. (c-d) Full FOV (top row) and reduced FOV (middle row) images for (c) bSSFP and (d) STFR. For closer inspection of the IV region, only the central 18x18 cm^2 region is shown, for four representative slices. The bottom row shows difference images between the full and reduced FOV reconstructions, indicating that STFR achieves superior OV suppression compared to bSSFP.

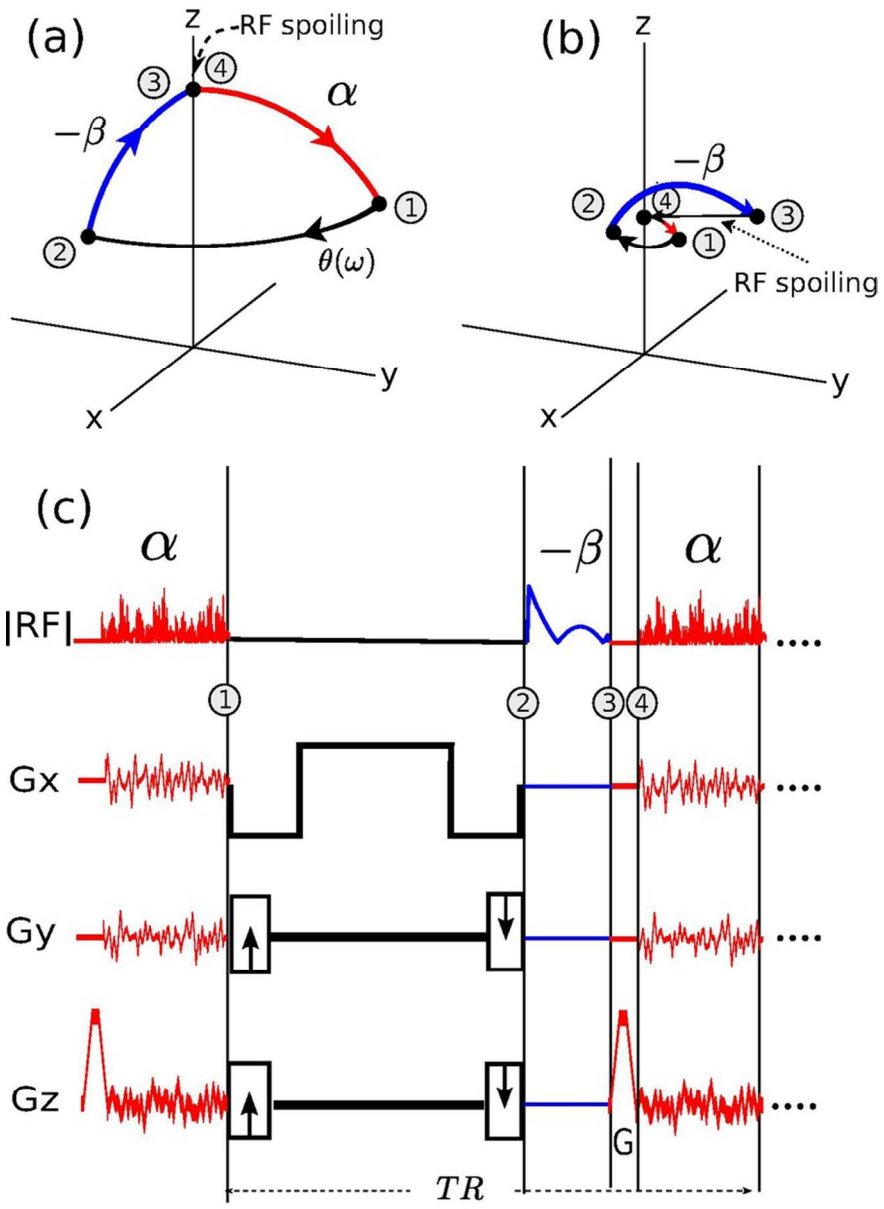

Figure 1: Proposed inner-volume-excitation STFR (IVex-STFR) sequence with 3D selective tip-down pulse (α) and spectral pre-winding tip-up pulse (-β). (a-b) Spin paths for (a) inner-volume (IV) and (b) outer-volume (OV) regions. (c) Schematic pulse sequence timing diagram. The IV excitation pulse tips the IV spins down toward the transverse plane (path 4->1 in Fig. (a)), after which the spin precesses with off-resonance frequency ω (1->2). After data readout, a non spatially selective tip-up pulse is played out, whose phase is nominally equal to the spin phase θ(ω) such that the spin is tipped back toward the longitudinal axis (path 2->3 in (a)). Outer-volume spins mainly experience the non spatially selective tip-up pulse (2->3 in Fig. (b)). However, since the IV excitation pulse can never be perfect, some direct OV excitation from the tip-down pulse (4->1) is inevitable. To avoid coherent steady-state signal from this small direct OV excitation, RF spoiling is used (12). The central point in this work is that the tip-up pulse in STFR helps to suppress the steady-state OV signal resulting from imperfect IV excitation pulses.

76x104mm (300 x 300 DPI)

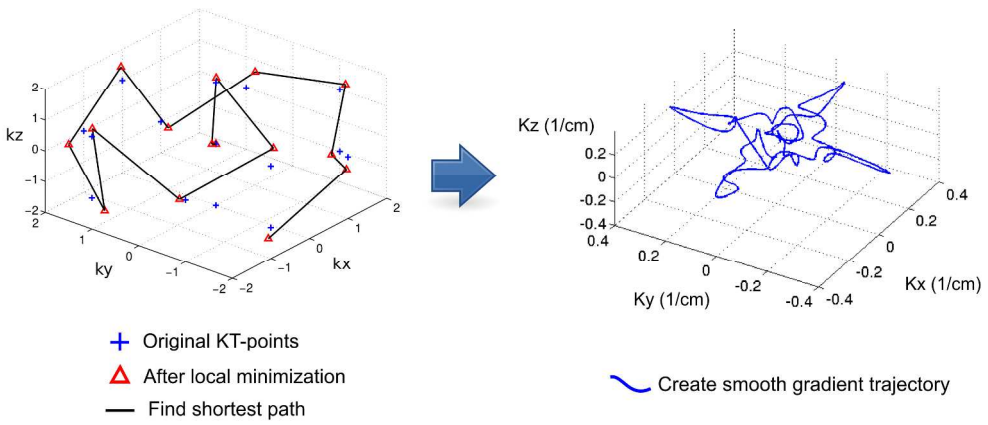

Figure 2: Summary of the 3D RF pulse design algorithm, first introduced in (10) and more recently in (11). We first obtain a KT-points trajectory (discrete "phase-encoding" locations in kx-ky-kz; blue "+" marks) using a modified orthogonal matching pursuit (OMP) approach (20). We then locally optimize the encoding locations using gradient-based algorithms (red triangles). We then determine the optimal visiting order for those phase encoding locations using a traveling salesman algorithm (22) (black straight line segments on left). Finally, we generate a continuous gradient waveform (right) that traverses those points using the method in (23), and design the RF pulse on this optimized k-space trajectory using iterative small-tip selective pulse design (28). In this example the target excitation is a rectangular box whose Fourier transform is a 3D sinc, and the final smooth k-space trajectory is concentrated in regions of 3D k-space where the Fourier transform of the target excitation is relatively large.

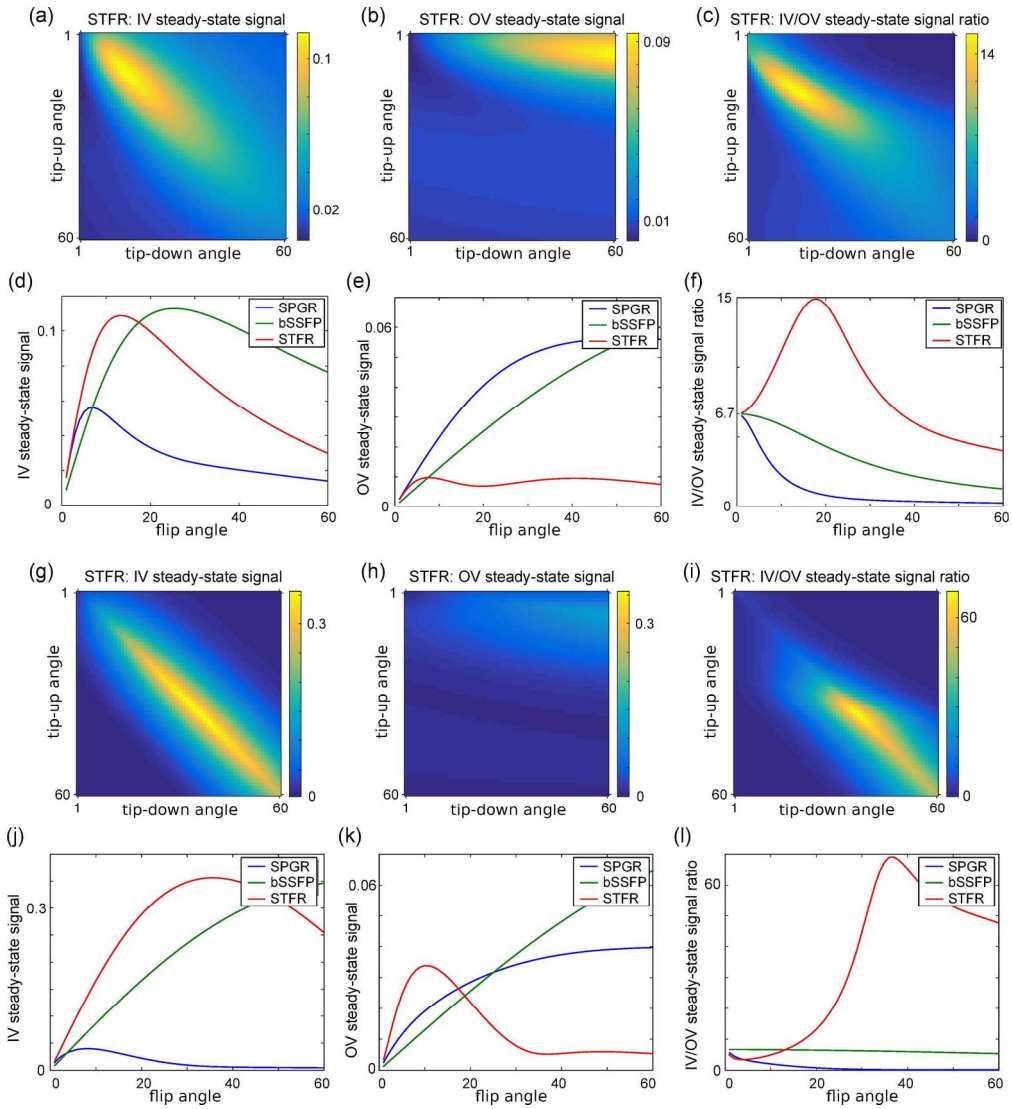

Figure 3: Simulated inner- and outer-volume steady-state signals and their ratio for STFR, bSSFP and SPGR. Results are shown for (a–f) white matter and (g–l) CSF. (a–c) STFR results for different tip-down and tip-up angle combinations, presented as 2D plots. Flip angles are in degrees. (d–f) Steady-state signal plots for SPGR and bSSFP, and for STFR with equal tip-down and tip-up angles. One-shot excitation in the outer-volume is 15% of the inner-volume, so an IV/OV steady state signal ratio larger than 1/0.15 (=6.7) means the sequence suppresses the OV signal, as seen for STFR. With the flip angles used in our first in vivo experiment (Fig. 4), the simulated IV/OV ratios for white matter is 2.0/4.0/11.9, for SPGR/bSSFP/STFR, respectively. (g–l) Corresponding results for CSF.

179x196mm (300 x 300 DPI)

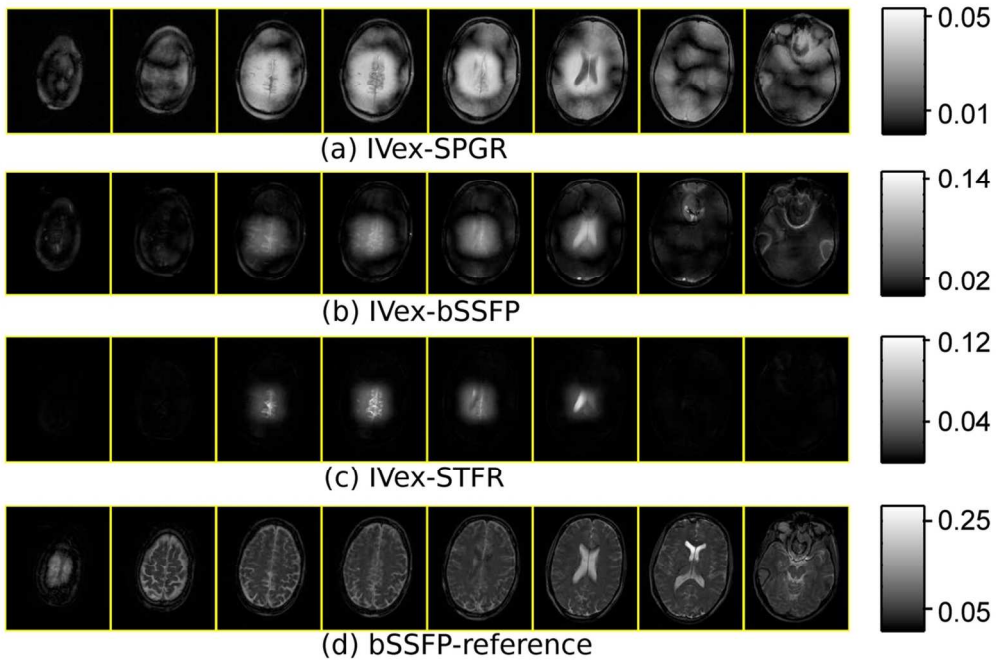

Figure 4: Steady-state brain imaging (a-c) with and (d) without inner-volume excitation, using a pulse sequence similar to that shown in Fig. 2(c). The target IV is a rectangular box. The gray scale is normalized by the maximum image value of each acquisition. The same eight slices are shown for (a) IVex-SPGR, (b) IVex-bSSFP, (c) IVex-STFR, (d) and conventional bSSFP. Balanced SSFP and STFR show similar tissue signal for inner-volume spins, but STFR has better OV suppression. The observed IV/OV ratios are 2.4/4.0/12.5 for IVex-SPGR/IVex-bSSFP/IVex-STFR, respectively, consistent with our simulations in Fig. 3.

111x74mm (300 x 300 DPI)

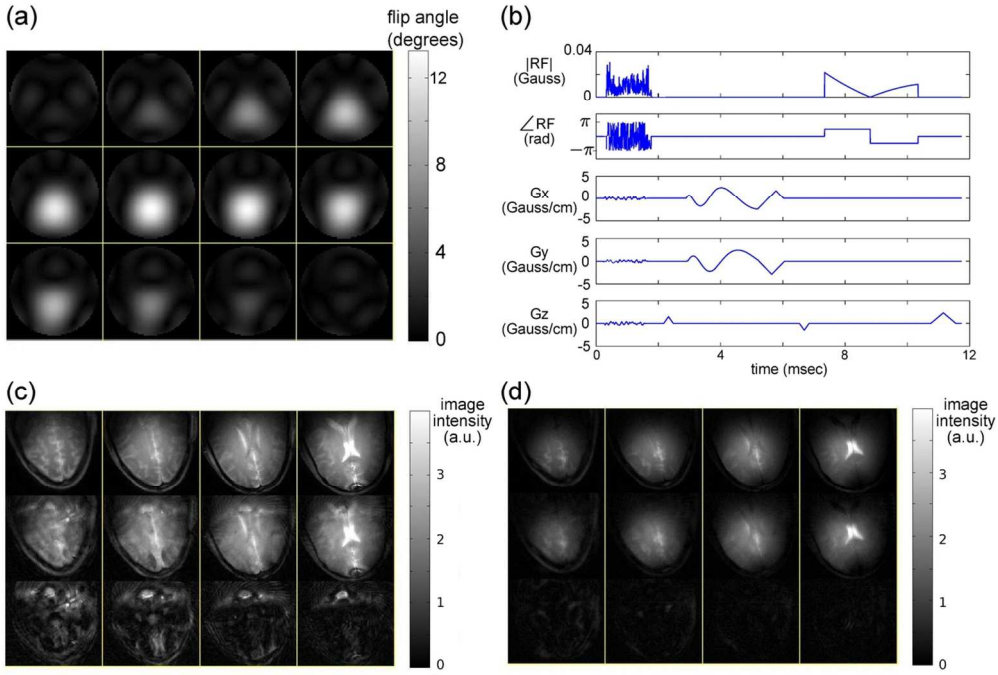

Figure 5: Stack-of-spirals rFOV imaging results for bSSFP and STFR, using a short (1.45 ms) "hockey puck" IV excitation. (a) Simulated magnetization produced by a single application of the IV excitation pulse. Twelve slices are shown. The short RF pulse produces a relatively blurred excitation pattern compared to the longer (4 ms) IV pulse in Fig. 4. The peak OV/IV excitation ratio is about 15% for this RF pulse. (b) STFR pulse sequence diagram, showing actual waveforms and sequence timing. (c-d) Full FOV (top row) and reduced FOV (middle row) images for (c) bSSFP and (d) STFR. For closer inspection of the IV region, only the central 18x18 cm2 region is shown, for four representative slices. The bottom row shows difference images between the full and reduced FOV reconstructions, indicating that STFR achieves superior OV suppression compared to bSSFP.

116x78mm (300 x 300 DPI)